Nonlinear global modes in hot jets

Lutz Lesshafft, Patrick Huerre, P. Sagaut, M. Terracol

HAL Id: hal-01023363
https://polytechnique.hal.science/hal-01023363

Nonlinear global modes in hot jets

By L U T Z   L E S S H A F F T[1,2], P A T R I C K   H U E R R E[1],
P I E R R E   S A G A U T[3] A N D M A R C   T E R R A C O L[2]

[1]Laboratoire d'Hydrodynamique (LadHyX), CNRS – École Polytechnique, 91128 Palaiseau, France

[2]ONERA, Department of CFD and Aeroacoustics, 29 av. de la Division Leclerc, 92322 Châtillon, France

[3]Laboratoire de Modélisation en Mécanique, Université Pierre et Marie Curie, Boite 162, 4 place Jussieu, 75252 Paris Cedex 05, France

Since the experiments of Monkewitz *et al.* (*J. Fluid Mech.* vol. 213, 1990, p. 611), sufficiently hot circular jets have been known to give rise to self-sustained synchronized oscillations induced by a locally absolutely unstable region. In the present investigation, numerical simulations are carried out in order to determine if such synchronized states correspond to a nonlinear global mode of the underlying base flow, as predicted in the framework of Ginzburg–Landau model equations. Two configurations of slowly developing base flows are considered. In the presence of a pocket of absolute instability embedded within a convectively unstable jet, global oscillations are shown to be generated by a steep nonlinear front located at the upstream station of marginal absolute instability. The global frequency is given, within 10 % accuracy, by the absolute frequency at the front location and, as expected on theoretical grounds, the front displays the same slope as a k^--wave. For jet flows displaying absolutely unstable inlet conditions, global instability is observed to arise if the streamwise extent of the absolutely unstable region is sufficiently large: while local absolute instability sets in for ambient-to-jet temperature ratios $S \leqslant 0.453$, global modes only appear for $S \leqslant 0.3125$. In agreement with theoretical predictions, the selected frequency near the onset of global instability coincides with the absolute frequency at the inlet. For lower S, it gradually departs from this value.

1. Introduction

Since the landmark investigations of Crow & Champagne (1971) and Brown & Roshko (1974), it has been generally acknowledged that high-Reynolds-number free shear flows such as circular jets, wakes and mixing layers are dominated by large-scale structures. The observed spreading rates are due in large measure to the streamwise development and interactions of these vortices (Winant & Browand 1974). It has also been well-established that the dynamics of free shear flows, including their spreading rate, may be manipulated or controlled by applying at the inlet low-level acoustic or mechanical excitations of appropriate frequency (see Ho & Huang 1982 and the review by Ho & Huerre 1984).

From the point of view of instability theory, vortical structures may be regarded in Fourier space as a collection of instability waves of distinct frequency and streamwise wavenumber. The above experimental observations very early on led theoreticians to adopt the so-called spatial stability approach, which consists of determining the complex wavenumber associated with each real frequency, as dictated by the linear

stability properties of parallel flows (Michalke 1965). A detailed review of spatial stability applied to parallel compressible circular jets is given in Michalke (1984). Such formulations have been successful in predicting the phase velocity, spatial growth rate and cross-stream distribution of low-intensity perturbations induced by external forcing. The generalization of these concepts to weakly non-parallel flows, in the framework of the WKBJ approximation, was first introduced for the case of incompressible circular jets by Crighton & Gaster (1976), and for the case of turbulent shear layers by Gaster, Kit & Wygnanski (1985). These analyses provided a systematic methodology to estimate the streamwise linear response of shear flows to forcing. In this setting, each shear flow is regarded as an amplifier of external perturbations, thereby reflecting its sensitivity to noise.

The legitimacy of this approach may only be assessed if one resorts to the concepts of absolute versus convective instability, first introduced by plasma physicists (Briggs 1964; Bers 1983). The application of these concepts to various configurations has led to the distinction between two main classes of shear flows: *noise amplifiers*, which are sensitive to external forcing, and *oscillators*, which beat at a specific intrinsic frequency. Flows that are convectively unstable at all streamwise stations have been shown to behave as noise amplifiers, whereas intrinsic oscillations only exist for flows displaying a region of absolute instability (see Huerre & Monkewitz 1990 and Huerre 2000 for comprehensive reviews). Co-flow mixing layers and constant-density jets belong to the former class, whereas the von Kármán vortex street behind a circular cylinder exemplifies an oscillator-type behaviour (Provansal, Mathis & Boyer 1987). Jets of sufficiently low density constitute yet another striking instance of shear flows displaying a transition from convective to absolute instability, as established theoretically by Monkewitz & Sohn (1988). The experiments of Monkewitz *et al.* (1990) demonstrated that self-sustained oscillations arise beyond the absolute instability onset in hot air jets. A similar behaviour was shown to occur in helium jets by Sreenivasan, Raghu & Kyle (1989), as further confirmed by Boujemaa, Amielh & Chauve (2004). In order to predict the frequency and spatial distribution of such self-sustained oscillations, it has proven fruitful to represent them as a *global mode*† consisting of an extended wavepacket which beats at a specific frequency (Chomaz, Huerre & Redekopp 1991 and Monkewitz, Huerre & Chomaz 1993). The objective of the present numerical study is to demonstrate precisely that the synchronized oscillations experimentally observed in hot jets may be ascribed to the presence of a nonlinear global mode induced by absolute instability.

The main findings of Monkewitz & Sohn (1988) and Monkewitz *et al.* (1990) may be summarized as follows. For a family of analytical velocity profiles which accurately represent experimentally measured mean flows in hot jets, absolute instabiliy arises when the ratio S of ambient-to-jet temperature falls below 0.72. For a top-hat inlet velocity profile typical of zero-Mach-number laboratory jets, the axisymmetric mode first exhibits a transition to absolute instability near the nozzle exit, at approximately 0.4 diameters away from the inlet. Furthermore, the experiments of Monkewitz *et al.* (1990) indicate that the critical value $S = 0.72$ very closely coincides with the appearance of synchronized oscillations. Two axisymmetric modes have been observed to arise with respective Strouhal numbers, based on jet diameter, $St = 0.3$ and $St = 0.45$.

---

† For clarity, we reserve the term *global mode* throughout this study to denote a wavepacket which is dominated by its upstream front dynamics, as opposed to self-sustained oscillations which may exist due to acoustic feedback.

The present investigation is largely motivated by recent advances which have been made in extending the theory of global modes to the fully nonlinear regime (see Chomaz 2005 for a review). The comprehensive analyses of Ginzburg–Landau evolution models by Chomaz (1992) and Couairon & Chomaz (1996, 1997a, b, 1999) have firmly established the intimate connection between nonlinear global modes and front velocity dynamics in systems giving rise to pattern formation. According to van Saarloos (1988, 1989), the velocity of the front separating the bifurcated state from the unperturbed basic state is governed by either linear or nonlinear mechanisms. In the former instance (Dee & Langer 1983), the front moves at a velocity such that, in the co-moving frame, the basic state is marginally absolutely/convectively unstable. In the latter instance, it is determined through a detailed phase-space analysis which must be carried out on a case-by-case basis. As in wake flows, it will be assumed for the present discussion that the front dynamics are governed by the linear selection criterion. In the context of Ginzburg–Landau equations on the semi-infinite interval $x > 0$, Couairon & Chomaz (1996, 1997a, b, 1999) have shown that the nonlinear global mode is dominated by a stationary front pinned at the upstream boundary $x = 0$. If the parameters are constant in x, the threshold for the appearance of a global mode coincides with the onset of absolute instability, and explicit scaling laws may be derived for its spatial structure. At threshold, the global frequency is given by the absolute frequency at the upstream boundary. In the context of Ginzburg–Landau equations with variable coefficients displaying a finite pocket of absolute instability in an infinite domain, Pier *et al.* (1998) and Pier, Huerre & Chomaz (2001) have demonstrated that the corresponding nonlinear global mode is also dominated by a stationary front, this time located at the upstream boundary of the absolutely unstable region. The global frequency is then given by the absolute frequency prevailing at this transition station.

Many of the results pertaining to Ginzburg–Landau models have been shown to also hold in real flow situations. Thus, the scaling law for the global spatial structure in semi-infinite media has been validated by Couairon & Chomaz (1999) in the case of the von Kármán vortex street simulations of Zielinska & Wesfreid (1995) and Wesfreid, Goujon-Durand & Zielinska (1996). The recent numerical simulations of synthetic parallel wakes in a semi-infinite domain by Chomaz (2003) very accurately follow the frequency selection criterion and the scaling law derived from Ginzburg–Landau models. The WKBJ formulation of Pier *et al.* (1998) in infinite media has been generalized to two-dimensional wakes by Pier & Huerre (2001). The vortex street frequency computed in a slowly varying streamwise-infinite wake is effectively given, within 2 % accuracy, by the absolute frequency at the convective/absolute instability boundary. More strikingly, this same criterion has been demonstrated by Pier (2002) to predict within 10 % accuracy the von Kármán frequency behind a circular cylinder for a range of Reynolds numbers between 100 and 200.

The experiments of Monkewitz *et al.* (1990) have shown that hot jets become self-excited as soon as absolute instability appears. However, it has not hitherto been demonstrated that the observed oscillations are due to the presence of a nonlinear global mode, associated with a front which imposes its absolute frequency on the entire jet. This issue constitutes the essential motivation for the present numerical investigation. Nichols, Schmid & Riley (2004) have recently presented direct numerical simulations of low-density jets in a low-Mach-number approximation, where acoustic waves are filtered out. The global frequency was shown to be close to typical absolute frequencies of the mean flow profiles in the presence of finite-amplitude fluctuations. The focus of our study is the nonlinear global mode structure of absolutely unstable

heated jets as predicted by the local instability properties of the underlying base flow profiles. We wish to emphasize that our main concern is not to reproduce all the detailed dynamics of hot jets in laboratory experiments. In the same spirit as Pier & Huerre (2001) and Chomaz (2003), we first seek to isolate and characterize the nonlinear global mode structure in a 'synthetic' hot jet configuration. As the studies of Monkewitz & Sohn (1988) and Monkewitz *et al.* (1990) indicate that absolute and global instability first sets in for axisymmetric perturbations, we restrict the analysis to a two-dimensional axisymmetric geometry, thereby avoiding the 'contamination' by secondary, symmetry-breaking helical instabilities. Additionally, in order to compare our results to the previous WKBJ analyses of Couairon & Chomaz (1996, 1997*a*,*b*, 1999), Pier *et al.* (1998) and Pier & Huerre (2001), we consider slowly varying base flows satisfying the boundary layer equations.

The outline of the study is as follows. The main physical assumptions and the equations governing the base flow and its perturbations are specified in §2, together with the linear instability concepts essential to the analysis. Section 3 presents the main features of the numerical methods used to obtain the base flow, to determine its linear instability properties, and to simulate the spatio-temporal evolution of perturbations. Self-excited oscillations are analysed and compared to nonlinear global mode theory in two distinct configurations. In §4, we examine the case of a base flow displaying a pocket of absolute instability embedded within convectively unstable surroundings. In §5, base flows with absolutely unstable inlet conditions are considered. These situations respectively correspond to the case of nonlinear global modes in infinite and semi-infinite media. The main results of the study are summarized and discussed in §6.

2. Problem formulation

Consider a laminar, subsonic, heated round jet emerging into an ambient fluid at rest. Its fundamental dynamics are assumed to be axisymmetric, and the problem is formulated in two-dimensional cylindrical coordinates r and x. The evolution of the flow is governed by the compressible, viscous equations of continuity, momentum and energy, cast in non-dimensional conservative flow variables $\boldsymbol{q} = (\rho, \rho u, \rho v, \rho E)$, where ρ and E denote density and total energy, and u and v are the axial and radial components of flow velocity $\boldsymbol{u}$. Together with the equations of state for a thermally and calorically perfect gas, the system is written in compact form as

$$\frac{\partial \rho}{\partial t} = -\mathrm{div}(\rho \boldsymbol{u}), \tag{2.1a}$$

$$\frac{\partial (\rho \boldsymbol{u})}{\partial t} = -\mathrm{div}\,(\rho \boldsymbol{u} \otimes \boldsymbol{u}) - \mathrm{grad}\ p + \mathrm{div}\ \boldsymbol{\tau}, \tag{2.1b}$$

$$\frac{\partial (\rho E)}{\partial t} = \mathrm{div}\left[-(\rho E + p)\boldsymbol{u} + \boldsymbol{\tau} \cdot \boldsymbol{u} + \frac{1}{Re\,Pr}\frac{\mathrm{grad}\ T}{(\gamma - 1)M^2}\right], \tag{2.1c}$$

$$p = \frac{1}{\gamma M^2}\rho T, \qquad E = \frac{T}{\gamma(\gamma - 1)M^2} + \frac{|\boldsymbol{u}|^2}{2}, \tag{2.1d,e}$$

with

$$\boldsymbol{\tau} = -\frac{2}{3Re}(\mathrm{div}\ \boldsymbol{u})\boldsymbol{I} + \frac{1}{Re}(\mathrm{grad}\ \boldsymbol{u} + \mathrm{grad}^T \boldsymbol{u}) \tag{2.2}$$

the viscous stress tensor for a Newtonian fluid, and p, T denoting pressure and temperature.

All quantities have been made non-dimensional with respect to the jet radius R, the centreline velocity U_c, density ρ_c and temperature T_c at the inlet. The viscosity μ and the thermal conductivity κ are assumed to be constant throughout the flow. The flow parameters defined in terms of dimensional quantities are: the Reynolds, Mach and Prandtl numbers $Re = \rho_c U_c R/\mu$, $M = U_c/c_c$ (with c_c the speed of sound on the centreline), $Pr = \mu c_p/\kappa$ (with c_p the specific heat at constant pressure), the ratio of ambient-to-jet temperature $S = T_\infty/T_c$, defined at the inlet, and the ratio of specific heats $\gamma = c_p/c_v$. Values of $Re = 1000$, $M = 0.1$, $Pr = 1$ and $\gamma = 1.4$ are retained for all cases presented.

The total flow variables are written as $q = q_b + q'$, where the perturbation components $q'(r, x, t)$ evolve within a steady base flow $q_b(r, x)$. The base flow is assumed to slowly develop in the streamwise direction, as in the case of sufficiently large Reynolds numbers. As in Pier & Huerre (2001), a family of base flow profiles is then sought in terms of primitive variables ρ_b, u_b, v_b and T_b, whose streamwise development depends on a slow coordinate $X = x/Re$:

$$\left. \begin{array}{ll} \rho_b(r, x) \sim \rho_0(r, X), & u_b(r, x) \sim u_0(r, X), \\ T_b(r, x) \sim T_0(r, X), & v_b(r, x) \sim Re^{-1}v_0(r, X). \end{array} \right\} \tag{2.3}$$

The $\sim$ symbol in (2.3) emphasizes the fact that such base states constitute a leading-order approximation for large Reynolds numbers $Re \gg 1$, satisfying the compressible boundary layer equations

$$\frac{\partial \rho_0 u_0}{\partial X} + \frac{1}{r}\frac{\partial}{\partial r}(r\rho_0 v_0) = 0, \tag{2.4a}$$

$$\rho_0 u_0 \frac{\partial u_0}{\partial X} + \rho_0 v_0 \frac{\partial u_0}{\partial r} = -\frac{\partial}{\partial r}\left(r\frac{\partial u_0}{\partial r}\right), \tag{2.4b}$$

$$T_0 = S + (1-S)u_0 + \frac{\gamma - 1}{2}M^2 u_0(1 - u_0), \tag{2.4c}$$

$$\rho_0 = T_0^{-1}. \tag{2.4d}$$

For unit Prandtl number and constant pressure, the energy equation has been replaced by the Crocco–Busemann relation (2.4c). This parabolic set of equations is integrated numerically, with X as the advancing variable. The boundary condition for the axial velocity at $X = X_0$ is given by the analytical profile of Michalke (1984)

$$u_0(r, X_0) = \frac{1}{2} + \frac{1}{2}\tanh\left[\frac{R}{4\theta}\left(\frac{1}{r} - r\right)\right], \tag{2.5}$$

with zero radial velocity, and with temperature and density profiles deduced from equations (2.4c) and (2.4d). The steepness of the profile is specified by the non-dimensional parameter R/θ, where θ is its momentum thickness. The slow variable X has been introduced for formal reasons only. In the presentation of the results, the base flow profiles will always be rescaled to the physical coordinate x.

If the right-hand side of (2.1a–c) is written in shorthand as the nonlinear operator $\mathrm{NL}(q)$, the perturbation equations for q' are expressed as

$$\frac{\partial q'}{\partial t} = \mathrm{NL}(q_b + q') - \mathrm{NL}(q_b). \tag{2.6}$$

This system is solved numerically without modelling assumptions. The only approximation made in the present study therefore arises from neglecting higher-order terms in Re^{-1} in the computation of the base flow. Under this assumption,

the temporal evolution of q' is computed exactly. This formulation also allows the investigation of perturbations evolving in parallel base flows, as in the validation case presented in §3.

In order to determine the local instability properties of the base flow, the Navier–Stokes equations (2.1) are recast in terms of primitive variables $q_p = (\rho, u, v, p)$ and linearized about the parallel flow q_b at a given frozen streamwise station X (Crighton & Gaster 1976; Huerre & Monkewitz 1990). Perturbations q'_p are then sought in the form of normal modes

$$q'_p(r, x, t) = Q(r) \exp{[i(kx - \omega t)]} + \text{c.c.}, \qquad (2.7)$$

with complex axial wavenumber k and complex angular frequency ω. The linear dispersion relation is expressed as a generalized eigenvalue problem in k with eigenfunction $Q(r)$, which is solved numerically as a function of ω, thereby leading to the determination of the spatial instability characteristics. As ω is allowed to be complex, this algorithm also serves to identify the complex absolute frequency ω_0 and wavenumber k_0, at which k^+- and k^--branches first pinch in the complex k-plane (Bers 1983).

3. Numerical methods and validation

The numerical scheme used for the integration of the boundary layer equations (2.4) is adapted from an algorithm described by Lu & Lele (1996). Starting from the inlet condition (2.5), radial profiles are obtained at successive streamwise locations. The momentum equation (2.4b) is discretized through a second-order Crank–Nicolson scheme, which yields a tridiagonal system in u_0. Boundary conditions $\partial u_0 / \partial r = 0$ on the axis and $u_0 = 0$ at the outer boundary point are imposed. The Crocco–Busemann relation and the equation of state can then be evaluated directly. The radial velocity v_0 is obtained by integration of the continuity equation along r, using an implicit Euler scheme, with $v_0 = 0$ as starting value on the axis. Since the equations are coupled, this procedure has to be iterated at each streamwise station until the profiles are converged. The algorithm has been validated against a self-similar solution of a compressible jet, derived by Pack (1954).

For the perturbation equations (2.6), spatial derivatives in both directions are evaluated with sixth-order-accurate centred explicit finite differences. A third-order Runge–Kutta algorithm is used for time advancement. Centred finite difference schemes are known to promote the growth of spurious oscillations of under-resolved wavelength. At each time step, these oscillations are dissipated by a selective tenth-order explicit filter scheme (Visbal & Gaitonde 2002), applied in both spatial directions, which uses an eleven-point stencil. The coefficients of the filter are defined locally, in order to preserve its high-order accuracy on non-uniform grids. The temporal and spatial schemes used in this study have been extensively tested in both aerodynamic and aeroacoustic applications by Terracol *et al.* (2005).

The perturbation equations are discretized on an orthogonal grid. Inside the 'physical' region, the spacing of grid points is kept constant in the axial direction ($\Delta x = 0.05$ for the cases presented in §4, $\Delta x = 0.1$ in §5), whereas in the radial direction, grid points are concentrated in the shear-layer region. The radial grid is the same for all cases presented, with a minimum spacing of $\Delta r = 0.008$ at $r = 1$, thereby resolving a shear-layer momentum thickness of $\theta = 0.1R$ by 12 grid points.

At the lateral and outflow boundaries, the physical domain is padded with sponge regions, where a damping term $-\lambda(r, x)q'$ is added to the right-hand side of the flow

equations (2.1*a–c*) (Colonius 2004), and grid stretching is smoothly increased up to a rate of 4 % from one point to the next. The purpose of these sponge regions is to minimize numerical box size effects by gradually attenuating all vortical and acoustic fluctuations before they reach the boundary of the computational domain. The damping coefficient $\lambda(r, x)$ increases smoothly from 0 to 1, according to the ramping function given by Chomaz (2003), over a distance $l_r = 150$ in the lateral sponge region and $l_x = 10$ in the outflow region. At the five outermost points nearest inlet, outlet and lateral boundaries, centred differentiation and filter schemes of decreasing stencil size are employed, and all fluctuations are set to zero at the lateral boundary and at the numerical outlet. Symmetry conditions $\partial(\rho, \rho u, \rho E)/\partial r = 0$, $\rho v = 0$ are imposed at $r = 0$ by mirroring the values of the flow variables onto five virtual points across the axis, whereby the stencil size of the high-order schemes can be retained. The coordinate singularity at $r = 0$ is avoided by placing the first radial grid point of the physical domain at half the local step size away from the axis.

At the inlet, non-reflecting characteristic boundary conditions developed by Giles (1990), and further discussed by Colonius, Lele & Moin (1993), are applied. At the first five computational points, which are not considered to be part of the physical region, the conservative flow variables are transformed to characteristic variables that represent incoming vorticity, entropy and acoustic waves and an outgoing acoustic wave. The incoming characteristics are either set to zero ('zeroth-order approximation'), or they are computed according to the first-order corrected formulation of Giles (1990), which takes into account oblique incidence of outgoing acoustic waves. This boundary treatment is not designed to specifically model nozzle effects, but to provide a Dirichlet condition for instability waves and prevent acoustic reflections. However, imperfections of the characteristic decomposition, which is based on the assumption of a uniform base flow normal to the boundary, may give rise to low-level vorticity perturbations that are excited by outgoing acoustic waves. This effect may be regarded as qualitatively similar to that of a hard nozzle in an experimental setting. In the computations presented in § 4, such perturbations are attenuated within an additional sponge zone at the inlet, extending over the interval $-8 \leqslant x < 0$, where the damping factor λ decreases from 1 to 0 over $-6 < x < 0$, and zeroth-order boundary conditions are imposed at $x = -8$. In the configurations studied in § 5, the need for an absolutely unstable and well-localized boundary precludes an inlet sponge zone. The first-order corrected boundary conditions are used in these cases.

For the numerical implementation of the linear instability analysis, a code developed by Olendraru & Sellier (2002) has been adapted to the heated jet case. The spatial eigenvalue problem is discretized via a Chebyshev collocation method, as elaborated by Khorrami, Malik & Ash (1989). An iterative search algorithm (Monkewitz & Sohn 1988) identifies the point k_0 in the complex k-plane where a k^+- and a k^--branch pinch. As a validation test, the results of Monkewitz & Sohn (1988) for the inviscid, zero-Mach-number limit have been successfully reproduced.

The accuracy of the numerical method used for the perturbation equations (2.6) is assessed by computing the linear impulse response of a parallel base flow. Nonlinear terms in $\boldsymbol{q}'$ are temporarily discarded from (2.6) for this calculation. A concentrated initial pulse of the form

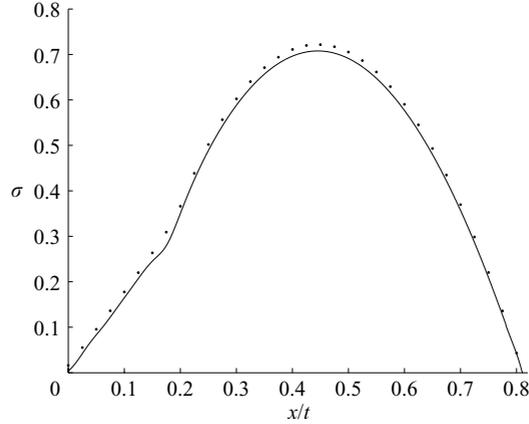$$u'_x(r, x, t = 0) = A \, \exp\left(-\frac{x^2 + (r-1)^2}{0.3^2}\right), \quad A = 10^{-30}, \tag{3.1}$$

FIGURE 1. Comparison of the growth rate σ along spatio-temporal rays x/t as obtained from the numerical simulation (—) and from the dispersion relation ($\cdot$) of a parallel jet with the parameters $R/\theta = 20$, $S = 0.57$, $Re = 500$ and $M = 0.1$.

is introduced into the jet shear layer in order to trigger the linear impulse response. According to linear theory, the fluctuations along a spatio-temporal ray x/t are then dominated for $t \to \infty$ by the most unstable linear mode with group velocity x/t and associated temporal growth rate σ (Huerre & Monkewitz 1990). Delbende, Chomaz & Huerre (1998) have proposed a method to evaluate $\sigma(x/t)$ from the numerically computed wavepacket at two distinct times. Results retrieved from the numerical simulation may then be compared to those obtained directly from the dispersion relation (Huerre & Rossi 1998), as displayed in figure 1. The numerical simulation is seen to accurately capture the linear instability properties of the base flow. In particular, the large disparity between the base flow and the perturbation amplitude (30 orders of magnitude) demonstrates that the formal separation into base flow and perturbation quantities has been rigorously preserved in the numerical implementation, so that perturbations are effectively resolved with full 64-bit machine precision. The slight offset between the two curves in figure 1 is attributed to the residual artificial dissipation introduced by the numerical method. Numerous tests have confirmed that this small underprediction of the absolute growth rate $\omega_{0,i}$ in the numerical simulation occurs systematically, whereas the real part $\omega_{0,r}$ of the absolute frequency is reproduced to even higher precision.

The base flow chosen for this validation test is close to marginal absolute instability, with an absolute growth rate $\omega_{0,i} = \sigma(x/t = 0)$ near zero. Note that figure 1 displays a clear discontinuity at $x/t = 0.18$, for results computed both from the dispersion relation and from the linear impulse response. A detailed examination of the pinching process indeed confirms that the same k^+-branch but different k^--branches are involved above and below $x/t = 0.18$. The mode which is associated with the absolute growth rate $\omega_{0,i}$ is seen to be different from the one exhibiting the maximum temporal growth rate $\omega_{i,max} = \sigma_{max}$. The characteristics of these two modes have been discussed in detail by Jendoubi & Strykowski (1994).

4. Nonlinear global mode in a jet with a pocket of absolute instability

In this section, we examine the properties of synchronized oscillations in a jet displaying a transition from convective instability at the inlet to absolute instability
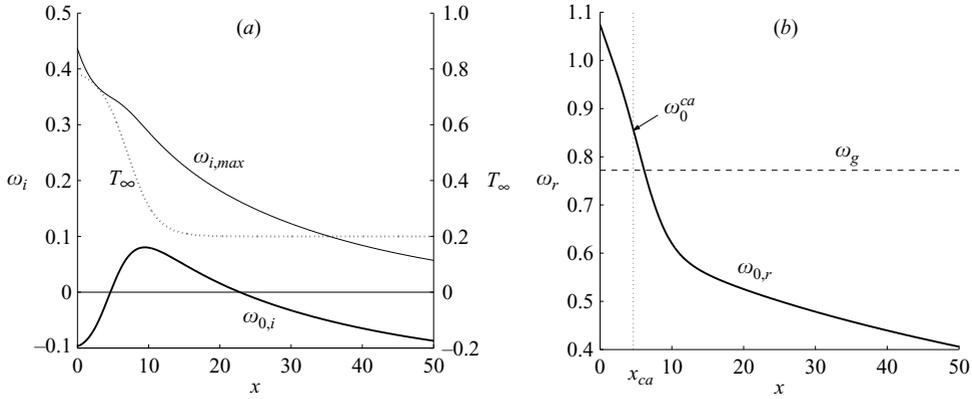
FIGURE 2. (*a*) Local absolute and maximum growth rates $\omega_{0,i}$ (—), $\omega_{i,max}$ (—) and ambient temperature T_∞ (· · ·) as a function of streamwise distance x. (*b*) Comparison of the local absolute frequency $\omega_{0,r}(x)$ (—) and the observed global frequency ω_g (- - -).

within a region of finite streamwise extent, in analogy with the synthetic wake of Pier & Huerre (2001). For this purpose, a base flow is conceived in which the streamwise development of the absolute growth rate $\omega_{0,i}$ is controlled by a prescribed variation of the ambient temperature $T_\infty(x)$ (figure 2*a*). The momentum thickness at the upstream boundary $x = 0$ of the physical region is taken to be such that $R/\theta = 11$. The computational grid consists of 430×1261 points in the radial and axial directions, with the physical region extending over $0 \leqslant r \leqslant 46$ and $0 \leqslant x \leqslant 50$. Tests on a grid of half the streamwise extent and without a lateral sponge zone have confirmed that the results presented here are not affected by the size of the computational box. We point out that in the presence of variations in the ambient temperature, the use of the Crocco–Busemann relation (2.4*c*) has been stretched beyond its strict limit of validity. This proved to be necessary in order to obtain an absolutely unstable pocket with a sufficiently pronounced convective/absolute upstream transition. Note that the viscous spreading of the base flow preserves the potential core over a much larger streamwise distance than is typical for mean profiles: in the present case, $u_0(0, x_{99}) = 0.99U_c$ is found at $x_{99} = 46$.

The streamwise variations of both $\omega_{0,i}$ and the maximum temporal growth rate $\omega_{i,max}$ are sketched in figure 2(*a*). The base flow is seen to be convectively unstable in an upstream region extending from the inlet to $x^{ca} = 4.63$. Owing to the decreasing temperature ratio, absolute instability prevails in the central region $x^{ca} < x < x^{ac}$, with $x^{ac} = 22.81$. Downstream of x^{ac}, the spreading of the jet induces a decrease of $\omega_{0,i}$ to negative values, and thus the flow returns to convective instability. Corresponding variations of the absolute frequency $\omega_{0,r}$ as a function of downstream distance are displayed in figure 2(*b*).

An initial pulse of the form (3.1) with amplitude $A = 10^{-3}$, introduced inside the absolutely unstable region at $x = 5$, gives rise, after a transient growth, to a synchronized periodic state at a global fundamental frequency ω_g. Figure 3 shows snapshots of the total azimuthal vorticity ω_θ over one cycle in the periodic regime. The flow is seen to be composed of regularly spaced ring vortices, which roll up at $x = 11$ and subsequently slowly decay further downstream. The diagram in figure 4 represents the synchronized oscillation of the radial velocity perturbation v' at the centre of the shear layer ($r = 1$) as a function of time and streamwise distance. The
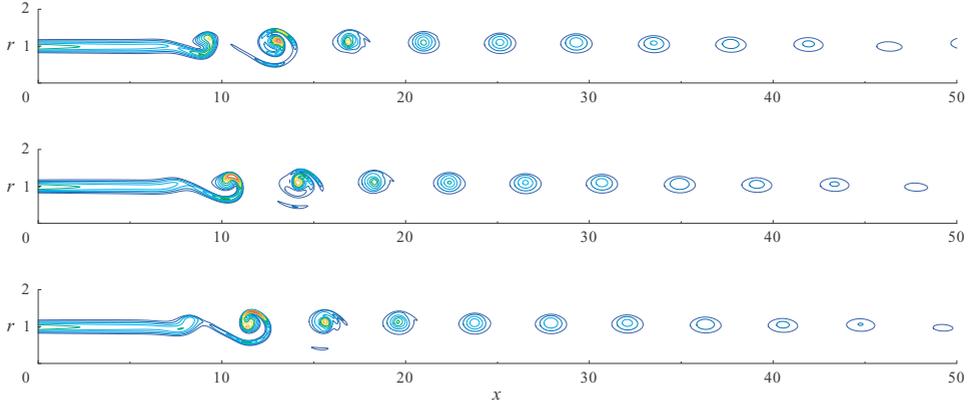
FIGURE 3. Total vorticity field $\omega_\theta(r, x)$ at three instants over one cycle in the periodic regime. Going from top to bottom, the snapshots are separated by one third of the cycle period.
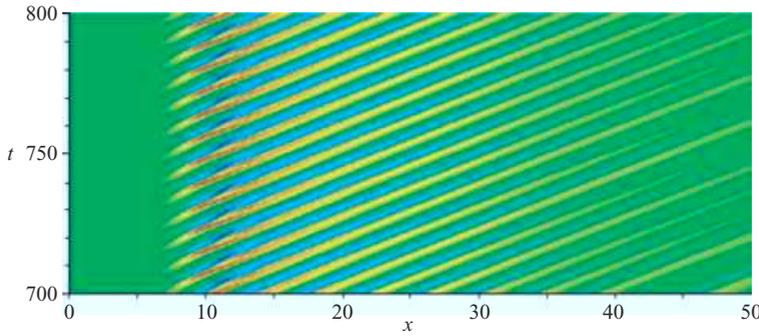

FIGURE 4. Spatio-temporal evolution of $v'(r = 1, x, t)$ in the periodic regime.

periodicity of the converged oscillatory state is clearly exhibited, as well as the absence of pairing interactions. As presented in figure 2(b), the observed global frequency is $\omega_g = 0.772$, to be compared with the theoretical value $\omega_0^{ca} = 0.857$ predicted by the frequency selection criterion of Pier *et al.* (1998).

The nonlinear global mode nature of the observed synchronized oscillations may also be ascertained by inspecting its spatial structure. According to Pier & Huerre (2001), the front that separates the bifurcated regime of saturated nonlinear oscillations from the unperturbed base state is located around the upstream point x^{ca} of marginal absolute instability. Upstream of x^{ca}, the tail of the global mode is then predicted to decay as a k^--wave.

In order to obtain a local measure of the amplitude at each streamwise station, the perturbation vorticity field $\omega_\theta'(r, x, t)$ is decomposed into the Fourier series

$$\omega_\theta'(r, x, t) = \sum_{n=-\infty}^{\infty} \Omega_n(r, x)\, e^{-in\omega_g t}, \qquad (4.1)$$

and an amplitude function $\eta_n(x)$ for each harmonic component is defined as the square root of its enstrophy integrated over r:

$$\eta_n(x) = \left(\int_0^{r_{max}} |\Omega_n(r, x)|^2 r\, dr \right)^{1/2}. \qquad (4.2)$$
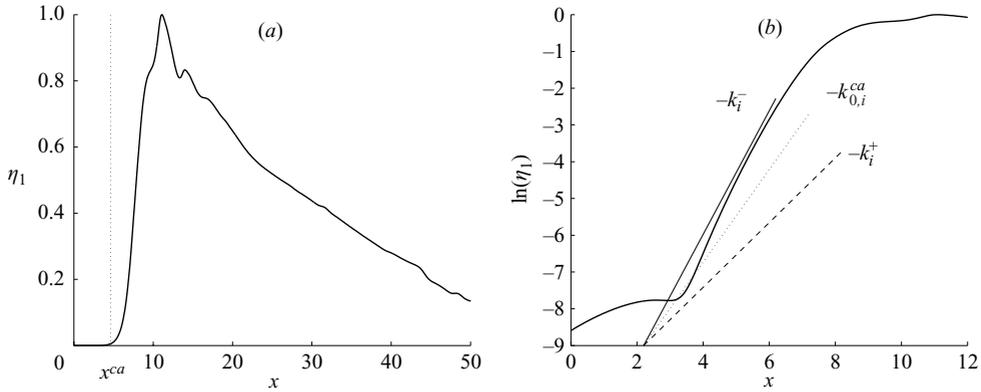
FIGURE 5. (a) Oscillation amplitude η_1 as a function of streamwise distance. (b) Semi-logarithmic plot of the upstream front region; comparison of the front slope with spatial growth rates $-k_{0,i}^{ca} = 1.26$, $-k_i^+(\omega_0^{ca}, x=4) = 0.88$ and $-k_i^-(\omega_0^{ca}, x=4) = 1.68$.

The resulting amplitude function $\eta_1(x)$ of the fundamental frequency ω_g is displayed in figure 5(a). A sharp upstream front is seen to occur in the vicinity of x^{ca}, followed by a maximum at the vortex roll-up station $x = 11$ and a slowly decaying nonlinear wavetrain further downstream. The spatial structure of the upstream front can be observed in detail in the semi-logarithmic diagram of figure 3(b). A region of exponential growth $\eta_1(x) \propto \exp(-k_i x)$ is clearly exhibited over the interval $3.5 < x < 7$. For $x < 3.5$, the front shape is masked by residual low-level vorticity disturbances likely to have been induced by the attenuation of upstream propagating acoustic waves within the numerical inlet sponge region. The spatial growth rates $-k_i^+(\omega_0^{ca})$ and $-k_i^-(\omega_0^{ca})$ at a typical station $x = 4$ in the upstream tail are also sketched in figure 5(b), together with the absolute spatial growth rate $-k_{0,i}^{ca}$. In the context of the signalling problem, the complex wavenumbers k^+, k^- are associated with instability waves propagating in the downstream and upstream direction, respectively. In figure 5(b), the slope of the envelope in the convectively unstable region $x < x^{ca}$ is seen to compare favourably with the k^- spatial growth rate, and to be quite distinct from its k^+ counterpart. This observation strongly indicates that the global oscillation is generated by a 'wave maker' within the flow, rather than by spurious forcing at the upstream boundary. The location of the front as well as its spatial structure correspond to the steep front scenario described by Pier & Huerre (2001), thus confirming that the observed oscillations indeed arise from the presence of a nonlinear global mode triggered by the pocket of absolute instability.

The global frequency $\omega_g = 0.772$ agrees reasonably well with the predicted value $\omega_0^{ca} = 0.857$. The 10 % discrepancy is of the same order of magnitude as in Pier (2002) for the cylinder wake. It is markedly narrower than the total variation in $\omega_{0,r}$ over the entire physical domain (figure 2b). Considering the steep streamwise variation of $\omega_{0,r}$ around x^{ca}, the accuracy of the criterion may be affected by the strong non-parallelism of the base flow. The effect of numerical dissipation, as discussed in §3, may also cause a slight shift of the transition station x^{ca} in the downstream direction, thereby lowering the effective value of ω_0^{ca}.

While the k^--nature of the front upstream of x^{ca} is apparent, the slope of $\eta_1(x)$ does not decrease to the absolute spatial growth rate $-k_{0,i}^{ca}$ at x^{ca}, as might have been expected. The observed front shape fails to adjust to this sharp decrease over a
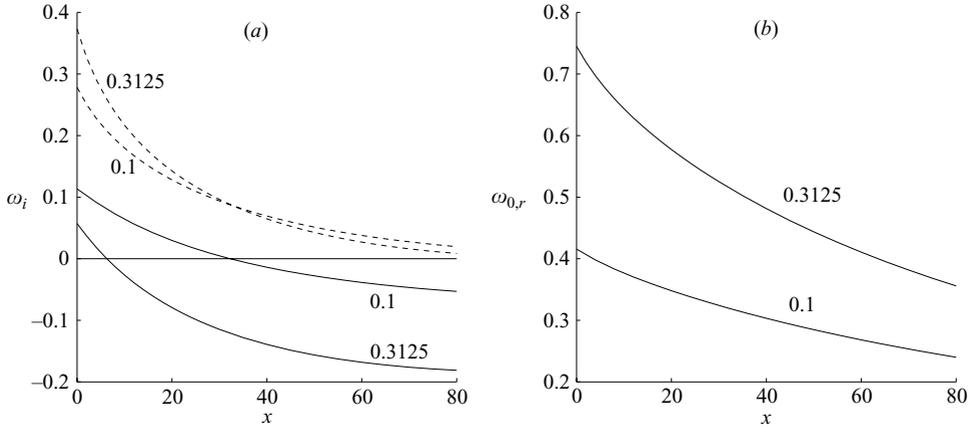
FIGURE 6. (a) Local absolute and maximum growth rates $\omega_{0,i}$ (——), $\omega_{i,max}$ (- - -) as functions of streamwise distance for $S = 0.3125$ and $S = 0.1$. (b) Corresponding absolute frequencies $\omega_{0,r}$.

distance much shorter than a single wavelength. Alternatively, the envelope slope may also be compared to the k^--branch corresponding to the observed global frequency ω_g instead of ω_0^{ca}: the branch $k^-(\omega_g, x)$, not displayed in figure 3(b), is then found to exhibit a slightly larger spatial growth rate and a smoother streamwise development than $k^-(\omega_0^{ca}, x)$, so that it reproduces more faithfully the observed envelope shape.

5. Nonlinear global modes in jets with absolutely unstable inlet

The configuration examined in the previous section, namely a pocket of absolute instability embedded within a convectively unstable flow, was designed by allowing for suitable streamwise variations of the ambient temperature T_∞. It is not typical of laboratory experiments such as those of Monkewitz *et al.* (1990). In this section, we examine the global dynamics of a family of hot jets with absolutely unstable inlet conditions, where T_∞ is kept constant along the stream. According to global mode theory in semi-infinite media (Chomaz 2005), the self-sustained oscillations are then expected to display a front which is pinned to the upstream boundary at $x = 0$, where the perturbation vorticity is imposed to be zero.

All base flows under consideration start from an initial momentum thickness such that $R/\theta = 10$, with temperature ratios S ranging from 0.1 to 1. In this range of parameters, a transition from upstream convective to downstream absolute instability within the jet is impossible: according to figure 6(a), the absolute growth rate is seen to decay monotonically with downstream distance. The streamwise variations of $\omega_{0,i}$ and $\omega_{i,max}$ are plotted for the least ($S = 0.3125$) and the most ($S = 0.1$) heated cases exhibiting self-sustained oscillations. All base flows in this range are seen to be absolutely unstable at the inlet. Corresponding curves for the absolute frequency $\omega_{0,r}(x)$ are given in figure 6(b).

The perturbation equations (2.6) are solved on a grid of 430×876 points in the radial and axial directions, respectively, the physical region extending over $0 \leqslant r \leqslant 46$ and $0 \leqslant x \leqslant 80$. Self-sustained oscillations induced by box size effects have been ruled out by conducting tests on shorter domains with physical regions $0 \leqslant x \leqslant 60$ and $0 \leqslant x \leqslant 40$. Grid independence has been demonstrated for $\Delta x = 0.05$ and $\Delta x = 0.1$, and the latter value has been retained for the present calculations.
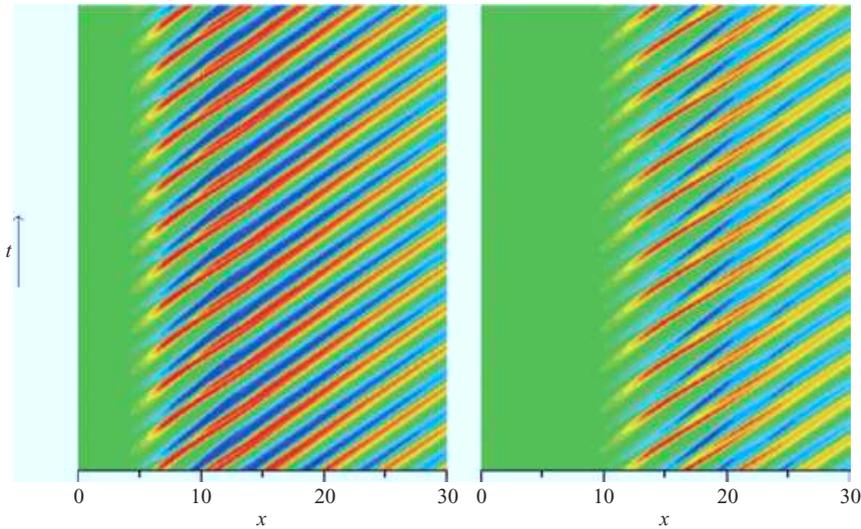
FIGURE 7. Spatio-temporal diagrams of $v'(r = 1, x, t)$ in the asymptotic regime over a time interval $\Delta t = 100$ for both modes observed at $S = 0.3$: (*a*) mode 1, (*b*) mode 2.
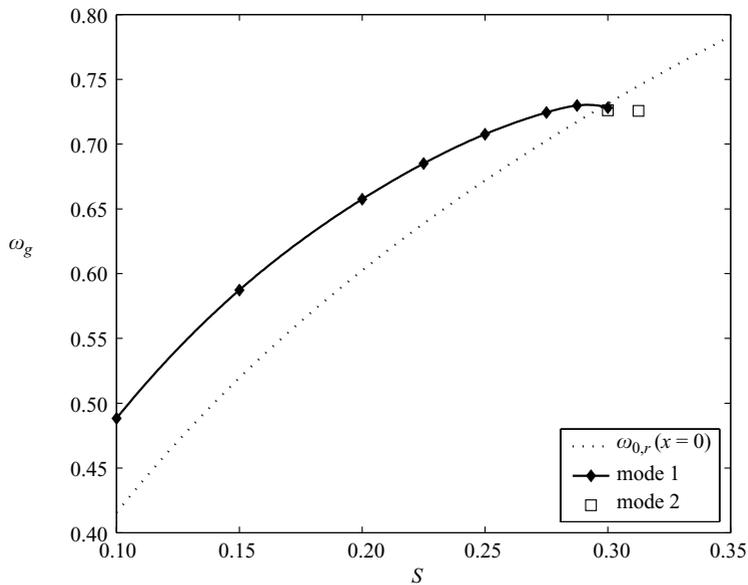

FIGURE 8. Global frequencies observed numerically at different values of S, compared to the absolute frequency at the inlet (dotted line).

Starting from an initial perturbation of the form (3.1) with $A = 0.01$, self-sustained oscillations are observed to develop for temperature ratios $S \leqslant 0.3$. The asymptotic states are characterized by the presence of ring vortices very similar to the ones displayed in figure 3. Typical spatio-temporal diagrams of the synchronized oscillations of the radial perturbation velocity v' at the centre of the shear layer are presented in figure 7. The periodicity of the asymptotic states is clearly exhibited.

The global frequencies observed for different values of S are represented in figure 8. These numerical results should be compared to the theoretical prediction

from global mode theory given by $\omega_{0,r}(x=0)$ (dotted line in figure 8). While local absolute instability at the inlet sets in as soon as S decreases below the transition value $S_{ca} = 0.453$, synchronized oscillations are observed numerically to persist only below the value $S_g = 0.3125$. The jet must therefore exhibit a sufficiently wide region of absolute instability, which is found to be of the order of one instability wavelength, in order to sustain a nonlinear front. In the range $0.325 \leqslant S \leqslant 1$, the wavepacket produced by the initial pulse is advected downstream, ultimately leaving only low-level residual fluctuations within the physical domain.

The most prominent feature in figure 8 is the presence of a branch of global frequencies, denoted 'mode 1' (solid line), covering the entire range $0.1 \leqslant S \leqslant 0.3$. At onset, the global frequency $\omega_g = 0.728$† of this mode coincides with the absolute frequency at the inlet $\omega_{0,r}(x=0) = 0.731$ (dotted line). The global frequency selection criterion derived by Couairon & Chomaz (1999), which predicts $\omega_g = \omega_{0,r}(x=0)$ in the vicinity of the global instability threshold, is therefore recovered. As S decreases, i.e. in the highly supercritical regime, ω_g departs from the absolute frequency. The spatio-temporal structure of mode 1 is illustrated in figure 5(*a*) at $S = 0.3$. Around $x = 9$, the shear layer rolls up into vortices, which are convected downstream without pairing. As S decreases, the vortex roll-up location of mode 1 moves towards the inlet.

Choosing as initial condition a weaker pulse (3.1) with an amplitude $A = 10^{-4}$ reveals the existence of another self-sustained oscillatory state ('mode 2', open squares in figure 8) for the specific values $S = 0.3$ and $S = 0.3125$. This mode is characterized by a vortex roll-up station located distinctly further downstream (compare figures 7*a* and 7*b*), outside the absolutely unstable region, while the global frequency stays within 3% of the absolute frequency at the inlet. As mode 2 is continued towards lower values of S, the front saturates within the absolutely unstable region, moves upstream, and mode 1 is recovered as the asymptotic state.

The simulation results are affected to some extent by the choice of the numerical upstream boundary conditions. Computations in which the first-order corrected conditions of Giles (1990) are replaced by a zeroth-order formulation yield a qualitatively similar behaviour of both modes, but the deviation of the mode 1 frequency from $\omega_{0,r}(x=0)$ is more pronounced for low values of S.

6. Concluding remarks

The occurrence of self-sustained synchronized oscillations in hot axisymmetric jets has been examined numerically for two distinct configurations, one displaying an absolutely unstable region embedded within a convectively unstable flow, the other starting from an absolutely unstable inlet. The results have demonstrated that in both cases these oscillations are the manifestation of a nonlinear global mode following the predictions from model analyses in infinite and semi-infinite domains, respectively.

In the case of an embedded pocket of absolute instability, the observed synchronized oscillations have been shown to be dominated by a steep nonlinear front, located at the convective/absolute transition station x^{ca} and decaying in the upstream direction as a k^--wave. The global frequency matches within 10% accuracy the absolute frequency at x^{ca}. This discrepancy is attributed to the non-parallelism of the flow induced by the streamwise gradient of the ambient temperature T_∞, which is required

† In the nearly marginal case $S = 0.3$ the calculations converge very slowly, and the asymptotic value of ω_g has therefore been obtained from computations in a shorter domain, with a physical region stretching over $0 \leqslant x \leqslant 40$.

in order to obtain a transition from convective to absolute instability within the flow. The location and the spatial structure of the front, as well as the global frequency, are in full agreement with the theoretical predictions pertaining to nonlinear global modes in an infinite domain (Pier *et al.* 1998, 2001).

We note at this point that, according to Monkewitz & Sohn (1988), an embedded pocket of absolute instability may also occur in jets with constant outside temperature for a narrow range of parameters. However, such a configuration presents considerable numerical difficulties, as it necessitates a very thin initial shear layer (R/θ well above 50 at the inlet). As a result, the flow is then prone to spurious acoustic forcing that may contaminate the global mode oscillations.

The simulations of flow configurations with constant ambient temperature and absolutely unstable inlet conditions have revealed the existence of two distinct synchronized oscillatory states close to the onset of global instability. One of these modes is seen to be dominant throughout the supercritical range of S, the other only being observed close to the global instability threshold $S_g = 0.3125$. At onset, the frequency of mode 1 coincides, within 0.4 % accuracy, with the absolute frequency at the inlet. For lower values of S, the global frequency gradually departs from $\omega_{0,r}(x=0)$. This result is in agreement with the Ginzburg–Landau model analysis of Couairon & Chomaz (1997*b*), according to which the $\omega_{0,r}(x=0)$ criterion only holds close to threshold, even in parallel flows. However, as soon as non-parallelism is present (Couairon & Chomaz 1999), a nonlinear front is only sustainable if its saturation takes place within the absolutely unstable region. In the present simulations, it has indeed been observed that the absolutely unstable region must be of sufficient streamwise extent in order to give rise to a nonlinear global mode. The non-parallelism of the base flow therefore accounts for the gap between local absolute instability onset at $S_{ca} = 0.453$ and global instability onset at $S_g = 0.3125$. As a result, the scaling law derived by Couairon & Chomaz (1997*b*) for parallel flows could not be recovered.

Self-sustained oscillations may also be present in the absence of absolute instability, which *a priori* precludes the onset of a global mode (Chomaz, Huerre & Redekopp 1988). For instance, constant-density jets may, under carefully tuned conditions, experience synchronized oscillations associated with a feedback loop consisting of a downstream propagating instability wave and an upstream travelling acoustic wave, preferentially emanating from vortex roll-up and pairing events (Laufer & Monkewitz 1980; Ho & Huerre 1984). This scenario has been observed, for instance, in the numerical simulations of convectively unstable, compressible jets carried out by Grinstein, Oran & Boris (1987). In our study, all calculations performed in the convectively unstable range $S > 0.453$ indicate that self-sustained oscillations induced by acoustic feedback do not arise for our parameter settings: vortex roll-up is observed not to give rise to synchronized oscillations, and vortex pairing never occurs in any of the asymptotic states presented. In the experiments of Monkewitz *et al.* (1990), however, vortex pairing was systematically present. Their parameter regime, which involves thinner initial shear layers and higher Reynolds numbers, remains to be investigated numerically.

REFERENCES

BERS, A. 1983 Space-time evolution of plasma instabilities – absolute and convective. In *Handbook of Plasma Physics* (ed. M. N. Rosenbluth & R. Z. Sagdeev), vol. 1, pp. 451–517. North-Holland.

BOUJEMAA, S., AMIELH, M. & CHAUVE, M. P. 2004 Analyse spatio-temporelle de jets axisymétriques d'air et d'hélium. *C. R. Mecanique* **332**, 933–939.

BRIGGS, R. J. 1964 *Electron-stream Interaction with Plasmas*. MIT Press. Cambridge, MA.

BROWN, G. L. & ROSHKO, A. 1974 On density effects and large structure in turbulent mixing layers. *J. Fluid Mech.* **64**, 775–816.

CHOMAZ, J.-M. 1992 Absolute and convective instabilities in nonlinear systems. *Phys. Rev. Lett.* **69**, 1931–1934.

CHOMAZ, J.-M. 2003 Fully nonlinear dynamics of parallel wakes. *J. Fluid Mech.* **495**, 57–75.

CHOMAZ, J.-M. 2005 Global instabilities in spatially developing flows: Non-normality and nonlinearity. *Annu. Rev. Fluid Mech.* **37**, 357–392.

CHOMAZ, J.-M., HUERRE, P. & REDEKOPP, L. G. 1988 Bifurcations to local and global modes in spatially developing flows. *Phys. Rev. Lett.* **60**, 25–28.

CHOMAZ, J.-M., HUERRE, P. & REDEKOPP, L. G. 1991 A frequency selection criterion in spatially developing flows. *Stud. Appl. Maths* **84**, 119–144.

COLONIUS, T. 2004 Modeling artificial boundary conditions for compressible flow. *Annu. Rev. Fluid Mech.* **36**, 315–345.

COLONIUS, T., LELE, S. K. & MOIN, P. 1993 Boundary conditions for direct computation of aerodynamic sound generation. *AIAA J.* **31**, 1574–1582.

COUAIRON, A. & CHOMAZ, J.-M. 1996 Global instability in fully nonlinear systems. *Phys. Rev. Lett.* **77**, 4015–4018.

COUAIRON, A. & CHOMAZ, J.-M. 1997a Absolute and convective instabilities, front velocities and global modes in nonlinear systems. *Physica* D **108**, 236–276.

COUAIRON, A. & CHOMAZ, J.-M. 1997b Pattern selection in the presence of a cross flow. *Phys. Rev. Lett.* **79**, 2666–2669.

COUAIRON, A. & CHOMAZ, J.-M. 1999 Fully nonlinear global modes in slowly varying flows. *Phys. Fluids* **11**, 3688–3703.

CRIGHTON, D. G. & GASTER, M. 1976 Stability of slowly diverging jet flow. *J. Fluid Mech.* **77**, 397–413.

CROW, S. C. & CHAMPAGNE, F. H. 1971 Orderly structure in jet turbulence. *J. Fluid Mech.* **48**, 547–591.

DEE, G. & LANGER, J. 1983 Propagating pattern selection. *Phys. Rev. Lett.* **50**, 383–386.

DELBENDE, I., CHOMAZ, J.-M. & HUERRE, P. 1998 Absolute/convective instabilities in the Batchelor vortex: a numerical study of the linear impulse response. *J. Fluid Mech.* **355**, 229–254.

GASTER, M., KIT, E. & WYGNANSKI, I. 1985 Large scale structures in a forced turbulent mixing layer. *J. Fluid Mech.* **150**, 23–39.

GILES, M. B. 1990 Nonreflecting boundary conditions for Euler equation calculations. *AIAA J.* **28**, 2050–2058.

GRINSTEIN, F. F., GLAUSER, M. N. & GEORGE, W. K. 1995 Vorticity in jets. In *Fluid Vortices* (ed. S. I. Green), pp. 65–94. Kluwer.

GRINSTEIN, F. F., ORAN, E. S. & BORIS, J. P. 1987 Direct numerical simulation of axisymmetric jets. *AIAA J.* **25**, 92–98.

HO, C.-M. & HUANG, L. S. 1982 Subharmonics and vortex merging in mixing layers. *J. Fluid Mech.* **119**, 443–473.

HO, C.-M. & HUERRE, P. 1984 Perturbed free shear layers. *Annu. Rev. Fluid Mech.* **16**, 365–424.

HUERRE, P. 2000 Open Shear Flow Instabilities. In *Perspectives in Fluid Dynamics* (ed. G. K. Batchelor, H. K. Moffatt, & M. G. Worster), pp. 159–229. Cambridge University Press.

HUERRE, P. & MONKEWITZ, P. A. 1990 Local and global instabilities in spatially developing flows. *Annu. Rev. Fluid Mech.* **22**, 473–537.

HUERRE, P. & ROSSI, M. 1998 Hydrodynamic instabilities in open flows. In *Hydrodynamics and Nonlinear Instabilities* (ed. C. Godreche & P. Manneville), pp. 81–294. Cambridge University Press.

JENDOUBI, S. & STRYKOWSKI, P. J. 1994 Absolute and convective instability of axisymmetric jets with external flow. *Phys. Fluids* **6**, 3000–3009.

KHORRAMI, M. R., MALIK, M. R. & ASH, R. L. 1989 Applications of spectral collocation techniques to the stability of swirling flows. *J. Comput. Phys.* **81**, 206–229.

LAUFER, J. & MONKEWITZ, P. A. 1980 On turbulent jet flows: a new perspective. *AIAA Paper* 80-0962.

LU, G. & LELE, S. K. 1996 A numerical investigation of skewed mixing layers. *Technical Rep.* TF-67. Department of Mechanical Engineering, Stanford University, Stanford, CA.

MICHALKE, A. 1965 On spatially growing disturbances in an inviscid shear layer. *J. Fluid Mech.* **23**, 521–544.

MICHALKE, A. 1984 Survey on jet instability theory. *Prog. Aerospace Sci.* **21**, 159–199.

MONKEWITZ, P. A., BECHERT, D. W., BARSIKOW, B. & LEHMANN, B. 1990 Self-excited oscillations and mixing in a heated round jet. *J. Fluid Mech.* **213**, 611–639.

MONKEWITZ, P. A., HUERRE, P. & CHOMAZ, J.-M. 1993 Global linear stability analysis of weakly non-parallel shear flow. *J. Fluid Mech.* **251**, 1–20.

MONKEWITZ, P. A. & SOHN, K. 1988 Absolute instability in hot jets. *AIAA J.* **26**, 911–916.

NICHOLS, J., SCHMID, P. J. & RILEY, J. J. 2004 Self-sustained oscillations in variable-density jets. *Bull. Am. Phys. Soc.* **49**, No. 9, 53.

OLENDRARU, C. & SELLIER, A. 2002 Viscous effects in the absolute-convective instability of the Batchelor vortex. *J. Fluid Mech.* **459**, 371–396.

PACK, D. C. 1954 Laminar flow in an axially symmetrical jet of compressible fluid, far from the orifice. *Proc. Camb. Phil. Soc.*, **50**, 98–104.

PIER, B. 2002 On the frequency selection of finite-amplitude vortex shedding in the cylinder wake. *J. Fluid Mech.* **458**, 407–417.

PIER, B. & HUERRE, P. 2001 Nonlinear self-sustained structures and fronts in spatially developing wake flows. *J. Fluid Mech.* **435**, 145–174.

PIER, B., HUERRE, P. & CHOMAZ, J.-M. 2001 Bifurcation to fully nonlinear synchronized structures in slowly varying media. *Physica* D **148**, 49–96.

PIER, B., HUERRE, P., CHOMAZ, J.-M. & COUAIRON, A. 1998 Steep nonlinear global modes in spatially developing media. *Phys. Fluids* **10**, 2433–2435.

PROVANSAL, M., MATHIS, C. & BOYER, L. 1987 Bénard-von Kármán instability: transient and forced regimes. *J. Fluid Mech.* **182**, 1–22.

VAN SAARLOOS, W. 1988 Front propagation into unstable states: marginal stability as dynamical mechanism for velocity selection. *Phys. Rev.* A **37**, 211–229.

VAN SAARLOOS, W. 1989 Front propagation into unstable states: II. linear versus nonlinear marginal stability and rate of convergence. *Phys. Rev.* A **39**, 6367–6390.

SREENIVASAN, K. R., RAGHU, S. & KYLE, D. 1989 Absolute instability in variable density round jets. *Exps. Fluids* **213**, 309–317.

TERRACOL, M., MANOHA, E., HERRERO, C., LABOURASSE, E., REDONNET, S. & SAGAUT, P. 2005 Hybrid methods for airframe noise numerical prediction. *Theoret. Comput. Fluid Dyn.* **19**, 197–227.

VISBAL, M. R. & GAITONDE, D. V. 2002 On the use of higher-order finite-difference schemes on curvilinear and deforming meshes. *J. Comput. Phys.* **181**, 155–185.

WESFREID, J. E., GOUJON-DURAND, S. & ZIELINSKA, B. J. A. 1996 Global mode behavior of the streamwise velocity in wakes. *J. Phys.* II *Paris* **6**, 1343–1357.

WINANT, C. D. & BROWAND, F. K. 1974 Vortex pairing, the mechanism of turbulent mixing-layer growth at moderate Reynolds number. *J. Fluid Mech.* **63**, 237–255.

ZIELINSKA, B. J. A. & WESFREID, J. E. 1995 On the spatial structure of global modes in wake flow. *Phys. Fluids* **7**, 1418–1424.